Plankton Benthos Res 16(1): 24–39, 2021

Plankton & Benthos Research

Primary production and plankton assemblages in the fisheries ground around San Jorge Gulf (Patagonia) during spring and summer

Valeria Segura[1,*], Ricardo I. Silva[1], Moira Luz Clara[1,2,3], Patricia Martos[4], Ezequiel Cozzolino[1] & Vivian A. Lutz[1,2]

[1] *Instituto Nacional de Investigación y Desarrollo Pesquero (INIDEP), Paseo Victoria Ocampo N° 1, B7602HSA. Mar del Plata, Argentina*
[2] *Instituto de Investigaciones Marinas y Costeras (IIMyC/CONICET), Rodríguez Peña 4046 Nivel 1, Casilla de Correo 1260, Correo Central, B7600. Mar del Plata, Argentina*
[3] *Instituto Franco-Argentino para el Estudio del Clima y sus Impactos (UMI-IFAECI/CNRS), Intendente Güiraldes 2160, C1428EGA, Buenos Aires, Argentina*
[4] *Universidad Nacional de Mar del Plata. Facultad de Cs Exactas y Naturales. Departamento de Ciencias Marinas, B7600. Mar del Plata, Argentina*

Received 9 May 2020; Accepted 20 September 2020 Responsible Editor: Tetsuichi Fujiki

doi: 10.3800/pbr.16.24

Abstract: The San Jorge Gulf, and the littoral to its north, is one of the most important fishing grounds for Argentina. Nevertheless, phytoplankton production has been scarcely studied. Here we analyzed during spring (2008) and summer (2009) the phytoplankton biomass, production, and the composition of phytoplankton and protozooplankton; their possible trophic relationships, and physical conditioners. At the south coast of the gulf during spring micro-nano-plankton (diatoms and dinoflagellates) were predominant and responsible for the maximum integrated production, comparable to that reported for the rich Argentinian shelf-break. Part of the organic carbon produced there was consumed by heterotrophic dinoflagellates, adding a trophic level to the food web. While at the center of the gulf, a conspicuous deep chlorophyll maximum would probably add organic matter to the bottom. During the following summer (2009), the ultrafraction represented the largest contribution to total phytoplankton biomass, and was dominated by *Synechococcus* sp. This, plus the abundance of ciliates, indicate the prevalence of a microbial food web during summer. It has been found that the frontal zones in the north and south of the gulf, favoring high phytoplankton biomass and its maintenance due to high primary production, provide a favorable food environment for impregnated female shrimp in spring, and for larvae during summer.

Key words: bio-optical properties, plankton assemblages, primary production, San Jorge Gulf, Southwestern Atlantic

Introduction

The sustainability of an ecosystem depends on the flow of energy between its components and is determined by its capacity to maintain a balance between the production and the loss of biomass in each of the trophic levels. Phytoplankton constitutes the base of the marine food webs, and in temperate seas some characteristics of the spring bloom-timing of initiation and duration, timing of peak and peak amplitude-will affect the larval survival and consequently the next year fish recruitment (Platt et al. 2003). An easy way to estimate the phytoplankton biomass is the chlorophyll *a* concentration, *Chla*. A recent satellite analysis of the last ~20 years reported a significant increase in surface chlorophyll in the Argentine continental shelf, with potential implications for trophic relationships and the reproductive success of fish populations (Marrari et al. 2017). Moreover, to evaluate the sustainability capacity of a system, it is necessary to know not only the biomass, but also the primary production, *PP* (e.g., Pauly & Christensen 1995). Although, there is a relationship between *Chla* and *PP*, it changes according to the different assemblages of

* Corresponding author: Valeria Segura; E-mail, vsegura@inidep.edu.ar

phytoplankton present in a place and the physiological status of the cells (Geider et al. 1986, Bouman et al. 2005, Segura et al. 2013).

There are not enough primary production estimations in the world ocean, in comparison with chlorophyll measurements, which are easier to perform; and only a fraction of these *PP* studies carried out production versus irradiance incubations (*P&E*). These experiments allow the derivation on the two main photosynthetic parameters, α^B (initial slope of production versus irradiance at low values, normalized by *Chla*) and P_m^B (maximum production at light saturation, normalized by *Chla*), which are inputs for satellite and biogeochemical models to estimate marine primary production.

The Argentine Sea has high concentrations of *Chla* according to ocean color satellite images (Gregg et al. 2005, Rivas et al. 2006) and seems to be highly productive according to results from global models (e.g., Longhurst et al. 1995). However, despite recent efforts there is still a scarcity of field data on primary production for this region of the South Atlantic (El-Sayed 1964, Mandelli 1965, Mandelli & Orlando 1966, El-Sayed 1968, Villafañe et al. 2004a, b, Schloss et al. 2007, Garcia et al. 2008, Lutz et al. 2010, Segura et al. 2013, Dogliotti et al. 2014, Lutz et al. 2018).

The San Jorge Gulf (SJG, ~45°S to 47°S) and the littoral to the north between Cape Dos Bahías and Rawson location (NL, ~43°S to 45°S) form part of the North Patagonia Ecosystem (between ca. 41°S and 48°S, and from the coast to the isobath of 100 m) (Fig. 1). There, important phytoplankton spring blooms, dominated by diatoms and dinoflagellate groups (Akselman 1996), have been observed associated with fronts (Akselman 1996, Carreto et al. 2007, Rivas et al. 2006). The SJG is an important fishing ground for Argentina being a focus of study since the 1980's by the National Fisheries Research and Development Institute (INIDEP) and having generated a broader interest as a priority marine area by the initiative "Pampa Azul" since 2014. The gulf has a diversity of habitats for feeding and reproduction of many species, several of them of great economic interest such as the Argentine red shrimp (Bertuche et al. 2000), Argentine hake (Bezzi et al. 1995), and the southern king crab (Wyngaard et al. 2016). The Argentine red shrimp represents one of the most profitable fisheries for the country and the annual landings have consistently increased since the year 2006; in 2013 its capture represented more than 40% of the total commercial species exported by Argentina (Moriondo Danovaro et al. 2016). The shrimp breeding season occurs during spring and summer with maximum intensity from November to March along the Patagonian littoral with focus along the coastal area from 42°S to 47°S (Moriondo Danovaro 2010, Fernández et al. 2012). The beginning of their reproductive activity is related to the formation of oceanographic fronts, where there is available food for the survival of the larvae (Carreto & Cuchi Colleoni 2001, Souto & Moriondo Danovaro 2019).

It is known that environmental changes immediately affect the lower levels of trophic webs (Legendre & Rassoulzadegan 1995) favoring either a classic (larvae grazing on large phytoplankton), a microbial (larvae feeding on small protozooplankton, which graze on small phytoplankton), or a multivorous (classic and microbial trophic webs) type. In the case of the Argentine red shrimp the critical period in the life cycle is the transition from nauplius to protozoea stage (planktonic), in which the larvae change from endogenous to exogenous feeding (Mallo & Fenucci 2004), grazing on large phytoplankton (diatoms and dinoflagellates) via a classic food web (Moriondo Danovaro et al. 2016).

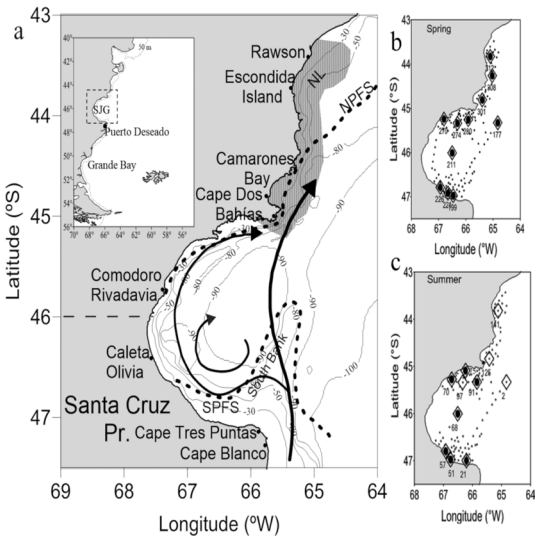

Fig. 1. (**a**) Map of bottom topography of the San Jorge Gulf (SJG) and north littoral (NL); lines mark a schematic representation of the Northern Patagonian Frontal System (NPFS) and the Southern Patagonian Frontal System (SPFS); and arrows depict the summer circulation (described in Matano & Palma 2018, and simplified in Dans et al. 2020). The grey painted area marks the littoral to the north of the gulf, NL. Location of the oceanographic stations in the (**b**) spring and (**c**) summer cruises. Symbols indicate the types of *in situ* samples collected for different studies: diamond: $PP+a_p(\lambda)+Chla$; black circle: plankton assemblages; and small dot: only *Chla.*

In order to better understand the base of the trophic food web in different zones of the SJG and NL during spring (2008) and summer (2009) the main aims of this study were: 1) to estimate the phytoplankton biomass (as *Chla* and carbon) and the primary production, 2) to characterize the plankton assemblages (phytoplankton and protozooplankton), and 3) to explore the relationship between these plankton properties.

Hydrography of the study area

The San Jorge Gulf (SJG) is a semicircular basin located in the Argentine sea between 45°S (Cape Dos Bahías) and 47°S (Cape Tres Puntas) and between ~65°30′W and 67°43′W. This shape and the strong persistent westerly winds favor coastal upwelling in certain regions of the gulf (Pisoni et al. 2018). The bottom topography is

relatively shallow with a depression located in the central region (~100 m) and a shoal named South Bank (Fig. 1a), contouring the 80 m isobath, that separates the southern portion of the gulf from the open shelf (Tonini et al. 2006, Matano & Palma 2018). The interaction between tidal currents and bottom topography near the South Bank generates a large tidal dissipation center (Palma et al. 2004, Tonini et al. 2006, Luz Clara et al. 2015, Palma et al. 2020).

The gulf has a wide connection with the Patagonian shelf that is occupied by shelf waters (salinities of 33.4–33.8), modified by the contribution of the low salinity waters of the Magellan Plume transported by the Patagonian Current (<33.4; Bianchi et al. 1982, Guerrero & Piola 1997). When reaching the southern tip of the gulf, these cold and less saline waters diverge into two branches: one flows into the SJG along the coast (onshore), while the other continues towards the north-east (Palma et al. 2004, Palma et al. 2020). The mean circulation is dominated by a cyclonic gyre bounded by a relatively strong coastal current and, on its offshore side, by the Patagonia Current (Matano & Palma 2018). The gulf circulation varies significantly with season, and a maximum in the onshore current strength has been observed in summer (Matano & Palma 2018). The north and south shallow depth (~30 m) extremes of the gulf are influenced by the presence of two frontal systems that differ in their main forcing, as well as in their temporal and spatial scales (Glorioso 1987, Bogazzi et al. 2005). The Northern Patagonian Frontal System (NPFS, Sabatini & Martos 2002), develops during austral spring and summer along the NL and enters into the northern half of the SJG. This is forced by seasonal thermal stratification and high tidal energy dissipation (Glorioso 1987, Sabatini & Martos 2002, Bogazzi et al. 2005). The Southern Patagonian Frontal System (SPFS, Bogazzi et al. 2005) is a permanent thermohaline front, characterized by the transition between coastal waters (tidally mixed, nutrient-rich and low salinity) (Guerrero & Piola 1997, Bogazzi et al. 2005) and continental shelf water (higher salinity and seasonally stratified).

Methods

Measurements

Field sampling took place in the SJG and the NL (from 43° to 47°S and from 65°W to the coast) on board the RV *Capitán Oca Balda*: spring cruise (OB03/2008; 20 November-11 December 2008) and summer cruise (OB01/2009; 21 January-11 February 2009) (Fig. 1b, c). A total of 122 oceanographic stations were occupied in the spring cruise and 113 stations in the summer one (Fig. 1b and c). At each of the stations, temperature and conductivity profiles were carried out using a CTD (SBE19); these data were processed, quality checked and stored in the Regional Oceanographic Data Base (BaRDO) at the Physical Oceanography laboratory of INIDEP.

At selected stations (see Fig. 1b and c) samples were collected at three depths: surface using a bucket and two other depths using Niskin bottles: one at the fluorescence maximum and another one below it (in spring); or one at the thermocline and another one below it (in summer, since no fluorescence sensor was available). When profiles were homogeneous, two intermediate depths in the water column were sampled. These water samples were used for the determination of the following variables:

a) In situ Chla (n=310 samples in spring and 324 in summer). After collection seawater samples were filtered under dim light and low pressure (35 kPa), onto Millipore APFF (GF/F) glass fiber filters. These filters were kept in liquid nitrogen (−196°C) on board and in an ultra-freezer (−86°C) in the laboratory until analysis. The fluorometric method of Holm Hansen et al. (1965) with modifications (Lutz et al. 2010) was used to determinate the *Chla* concentration.

b) Particulate absorption coefficients (n=21 in both spring and summer cruises). A known volume of water samples (300 ml) were filtered under dim light and low pressure (35 kPa), onto Millipore APFF (GF/F) glass fiber filters, which were then placed flat (particles facing up) on histology-type cassettes, kept in liquid nitrogen (−196°C) on board and in an ultra-freezer (−86°C) in the laboratory until analysis. Once in the laboratory, the quantitative filter technique (Mitchell 1990) was used to determine the absorption spectrum of total particles ($a_p(\lambda)$) and the method of Kishino et al. (1985) for the non-algal particles ($a_{NAP}(\lambda)$) using a UV-2450 Shimadzu spectrophotometer with an integrating sphere; the coefficients of Hoepffner & Sathyendranath (1992) were used to account for the path-length amplification factor. Then, the absorption coefficient of phytoplankton ($a_{Ph}(\lambda)$) was estimated by subtracting $a_{NAP}(\lambda)$ from $a_p(\lambda)$ absorption coefficients. The specific absorption coefficient of phytoplankton at 440 nm (a^B_{ph} (440)) was obtained through normalizing by *Chla*.

c) Primary Production (n=11 each in spring and summer). The method used was that proposed by Hama et al. (1983), as detailed in Lutz et al. (2010). A surface seawater sample was inoculated with a solution of $NaH^{13}CO_3$ to a final enrichment of 8.02%, dispensed into 17 bottles (500 ml square polycarbonate Nalgene): 15 of them set at different light intensities from E ~1.28 to 950 μmolquanta $m^{-2}s^{-1}$ (measured within each bottle with a Biospherical QSL-100 radiometer) and one in the dark (as a control), and incubated for 3 hours in a "*production & irradiance box*" (*P&E*), with halogen lamps and the aid of a circulating bath to maintain the temperature as it was at the site of collection. A known volume of sample (between 200 ml to 300 ml) not inoculated was filtered at the beginning of the experiment for the determination of natural ^{13}C abundance in the water. After the incubation, each bottle was filtered onto pre-combusted Whatman GF/F glass-fiber-filters. The volume of filtration varied between 200 ml and 350 ml depending on the color of material above the

filter. The filters were stored dry; in the laboratory they were fumed with *HCl* and encapsulated. The amount of particulate organic carbon and the ^{13}C in the sample was analyzed on an Elementar Vario Micro Cube elemental analyzer (Elementar Analysensysteme GmbH, Hanau, Germany) interfaced to a PDZ Europa 20-20 isotope ratio mass spectrometer (Sercon Ltd., Cheshire, UK) at UC Davis Stable Isotope Facility. The assimilated carbon in each sample, p (mg C m^{-3} h^{-1}) was computed according to Hama et al. (1983), Collos & Slawyk (1985) and Fernández et al. (2005). The value of the abundances of total dissolved inorganic carbon (DIC) in the natural seawater used was 2400 μmol L^{-1}(Collos, personal communication) and the % atom ^{13}C in DIC was 1.11%. The exponential equation of Platt et al. (1980) was used to fit the curve of production versus irradiance (*P&E*) and to calculate the main photosynthetic parameters: α and P_m. The value of α was corrected for the spectrum of the lamp and the absorption coefficient of phytoplankton according to Dubinsky et al. (1986). These parameters were normalized by the *Chla* determined for the surface at that place ($Chla_{sPP}$) to obtain: α^B (mg C (mg *Chla*)$^{-1}$ h^{-1} (W m^{-2})$^{-1}$) and P_m^B (mg C (mg Chla)$^{-1}$ h^{-1}). The instantaneous primary production at the surface at noon, p_0 (mg C m^{-3} h^{-1}) and daily water-column integrated production, $P_{Z,T}$ (mg C m^{-2} d^{-1}) were calculated at each station following the parameterization of Platt et al. (1980, 1990); due to logistic restrictions *P&E* incubations were performed only for surface samples and were collected at different times of the day at the different stations (according to the cruise schedule); hence, the photosynthetic parameters were treated as being constant with depth and throughout the day. The maximum quantum yield of photosynthesis was computed as $\emptyset_m = f^*\alpha^B/\bar{a}_{ph}^B$; where $\bar{a}_{ph}^B$ is the spectrally averaged (400–700 nm) specific absorption coefficient of phytoplankton, and f is a factor 0.023 to account for the conversion of mg into moles of C, μmoles into moles of quanta, and hours into seconds (Kirk 2011, Bouman et al. 2018).

d) Phytoplankton and proto-zooplankton communities. Surface seawater samples (250 ml) were preserved with neutralized formaldehyde (0.4% final concentration) for phytoplankton and proto-zooplankton analysis (Throndsen 1978). An aliquot of 50 ml was stained by two fluorochromes: DAPI (to mark DNA) and proflavin (to mark the cellular membrane) using the method of Verity & Sieracki (1993) and then filtered onto a black polycarbonate membrane with pore size of 0.2 μm using low pressure; then mounted on slides with immersion oil and preserved at −20°C to study the ultra-plankton class size (*Ultra*, cells <5 μm). A combination of classic and fluorescence microscopic methods (Olympus IX 70 microscope) was used to identify and quantify the phytoplankton and proto-zooplankton communities from 0.2 μm to 200 μm size. *Ultra* was identified and enumerated using a fluorescence microscope with blue, green and ultraviolet filters to allow characterization of autotrophic and heterotrophic cells (Verity & Sieracki 1993). Cells belonging to nano-plankton (*Nano*, 5–20 μm) and micro-plankton (*Micro*, 20–200 μm) class sizes were identified and quantified using the sedimentation technique with an inverted microscope (Hasle 1978, Tomas 1997). Cell dimensions were measured throughout the counting procedure through analysis of images. Plankton cell volumes, V, (μm^3) were calculated by assigning simple geometric shapes to each species according to Hillebrand et al. (1999). The V were converted into carbon content, hereafter called biomass in terms of carbon, B_C (mg C m^{-3}) using different carbon-to-volume ratios for the different groups (Borsheim & Bratbak 1987, Put & Stoecker 1989, Menden Deuer & Lessard 2000).

The Shannon index (H'), commonly used as a measure of species evenness (Shannon & Weaver 1949), was estimated to evaluate the diversity. H' is a measure of the relative abundance of each species within a sample and is defined as

$$\left[H' = -\sum_{i=1}^{S} pi \log\ pi \right],$$

where pi is the proportion of the total plankton biomass of taxa i and S is the total plankton biomass.

e) Photosynthetically Active Radiation (*PAR*). Irradiance values crucial for the computation of *PP* were estimated as follows: The values of *PAR* irradiance at the surface, E_s, were continuously monitored during the cruise using a LI-COR cosine sensor. Following our previous work (Lutz et al. 2010), the study area was divided every 2° into latitudinal ranks (*LR*), and in turn each one was divided every 2 h (during daylight) into different hour-ranks (*HR*). The average E_s from all the measurements recorded by the continuous sensor within the same *LR* and *HR* were calculated and assigned to the stations according to their location (to which *LR* they belonged). The downwelling attenuation coefficient of light, K_d (*PAR*), was computed using the model of Sathyendranath & Platt (1988). Then, these values were used to calculate the PAR downwelling irradiance profiles (E_Z).

f) Chlorophyll profiles. The continuous *Chla* profile in the water-column for all the station ($Chla_z$) and for the *PP* station ($Chla_{zPP}$) was estimated from the fluorescence profile (*Fl*) and the discrete measurements of *Chla* in spring. In summer (OB01/2009) a linear fitting to the discrete *Chla* values was used to obtain the continuous *Chla* profile since the *in situ* fluorometer was not available.

g) Water column stability. To determine the location of ocean fronts, the stability Simpson parameter (φ; see list of symbols in Table 1) was estimated (Simpson 1981). This is a measure of the mechanical work required to vertically mix the water column, and is defined as

$$\left[\phi = \frac{g}{h} \int_{-h}^{0} (\rho - \rho_0) \cdot z \cdot dz \right]$$

where g is the gravity, h is the depth, and ρ_0 is the mean

Table 1. List of symbols and abbreviations used with their description and units.

Notation	Description	Units
$a_{NAP}(\lambda)$	Absorption coefficient of non-algal particles at wavelength (λ)	m^{-1}
$a_{ph}^{B}(440)$	Specific absorption coefficient of phytoplankton at 440 nm wavelength	m^2 (mg *Chla*)$^{-1}$
$a_p(\lambda)$	Absorption coefficient of total particulate matter at wavelength (λ)	m^{-1}
α	Initial slope of production versus irradiance (at low values)	mg C h^{-1} (W m^{-2})$^{-1}$
α^B	Initial slope of production versus irradiance (at low values) normalized by *Chla*	mg C (mg *Chla*)$^{-1}$ h^{-1} (W m^{-2})$^{-1}$
B_C	Biomass of phytoplankton in terms of carbon	mg C m^{-3}
^{13}C	Isotope of Carbon 13	
Chla	Chlorophyll *a* concentration at a discrete depth	mg m^{-3}
$Chla_s$	Chlorophyll *a* concentration at the surface	mg m^{-3}
$Chla_{sPP}$	Chlorophyll *a* concentration at the surface coincident with *PP* estimations	mg m^{-3}
$Chla_{ZPP}$	*Chla* integrated in the water-column coincident with *PP* estimations	mg m^{-2}
$Chla_Z$	*Chla* integrated in the water-column	mg m^{-2}
$Chla_{sat}$	Satellite chlorophyll *a* concentration	mg m^{-3}
DCM	Deep Chlorophyll Maximum	m
E_s	Irradiance in the visible range at surface	μmol quanta m^{-2} s^{-1}
E	Irradiance	μmol quanta m^{-2} s^{-1}
E_Z	Irradiance in the visible range at depth z	μmol quanta m^{-2} s^{-1}
Fl	In vivo Fluorescence	relative fluorescence units
H'	Shannon index	
HR	Hour ranks	
$K_d(PAR)$	Diffuse attenuation coefficient for downwelling irradiance in the PAR	m^{-1}
LR	Latitudinal ranks	
Micro	Micro-plankton class size (cells >20 μm)	
Nano	Nano-plankton class size (cells from 2.0 to 20 μm)	
Phyto	Phytoplankton	
Proto	Proto-zooplankton	
p	Assimilated carbon	mg C m^{-3} h^{-1}
PAR	Photosynthetically Active Radiation (400–700 nm)	
PC	Plankton community	
PP	Primary production	
p_0	Instantaneous primary production at surface at noon	mg C m^{-3} h^{-1}
P_m	Maximum production at saturating irradiance	mg C h^{-1}
P_m^B	Maximum production at saturating irradiance normalized by *Chla*	mg C (mg *Chla*)$^{-1}$ h^{-1}
$P_{Z,T}$	Integrated daily water column primary production.	mg C m^{-2} d^{-1}
SSS	Surface Seawater salinity	practical salinity units
SBS	Bottom seawater salinity	practical salinity units
SST	Surface seawater temperature	ºC
SBT	Bottom seawater temperature	ºC
$\emptyset_m$	Maximum quantum yield of photosynthesis	mol C mol quanta^{-1}
φ	Stability parameter of Simpson	J m^{-3}
Ultra	Ultra-plankton class size (cells <5 μm)	
V	Plankton cell volumes	μm^3
Z	Depth of the station	m

density of the water column. Small values of φ indicate poorly stratified waters while high values are associated with stratified ones. In this work, the value of 40 J m^{-3} was used as the limit between homogeneous (φ<40) and stratified (φ>40) waters, as established by Sabatini & Martos (2002). Ocean Data View (ODV; Schlitzer 2018) software was used to convert the hydrographic data sets into a format readable by the DIVA (Data-Interpolating Variational Analysis) software, that allows one to spatially interpolate (or analyze) those observations on a regular grid in an optimal way.

h) Satellite chlorophyll, $Chla_{sat}$. Level 3 Aqua-MODIS satellite images (4 km spatial resolution and 8 days temporal resolution) were downloaded from the NASA ocean

color website (https://oceandata.sci.gsfc.nasa.gov/). The $Chla_{sat}$ values were obtained by averaging a 3×3 pixel window around the pixel closest to the sampling stations (Bailey & Werdell 2006).

Results

Physical properties

Spring 2008: Sea surface temperature (*SST*) ranged from 10.2 to 14.9°C, while sea bottom temperature (*SBT*) varied from 7.1 to 12.9°C. At the surface, low values were observed in the south-western and south-eastern sectors of the gulf, while maximum values were observed at the northwest, inside the gulf, and the NL (Fig. 2a). At the bottom, low values of temperature (*SBT*) occurred in the middle of the gulf, and higher values were observed in the north and south ends of the gulf (Fig. 2b). The range of sea surface salinity (*SSS*) varied from 33.0 to 33.5 with the maximum values in the center of the basin and towards the north, and the minimum values in the south coast and over the South Bank (Fig. 2c). The sea bottom salinity values (*SBS*) varied from 32.9 to 33.4 with a spatial distribution similar to that at the surface (Fig. 2d). The Simpson's parameter allowed identification of the location of the frontal regions: one in the southern coast extending over the South Bank (SPFS) and another on the north (NPFS) of the gulf to 44°S which, according to the φ value, was cut and reappeared as a third small front at the region of Isla Escondida (43.7°S) in the NL (Fig. 2e).

Summer 2009: The *SST* ranged from 13.6 to 18.3°C, and the *SBT* from 7.4 to 16.2°C. At the surface, minimum values were located at the South Bank, while at the bottom low values were distributed in the central region of the SJG (Fig. 3a and b). Salinity oscillated from 33.0 to 33.5 at the surface, and from 33.0 to 33.4 at the bottom; its distribution was similar at both depths, with the highest values in the north of the gulf and the lowest ones at the southern end extending over the South Bank (Fig. 3c and d). The Simpson's parameter marked again the presence of the two oceanic fronts, the one located in the southern region (SPFS) and the other extending from the north (NPFS) of the SJG and to the NL (Fig. 3e).

Characterization of the spring bloom development and demise

Distribution of $Chla_{sat}$ in spring showed high values associated with frontal regions, external regions and the NL, and low values at the center of the gulf. The maximum value of $Chla_{sat}$ was 9.03 mg m^{-3}, located at the NL, while the minimum value was 0.30 mg m^{-3}, at the center of the gulf (Fig. 4e). A succession of satellite images from prior, during and after the cruise indicate that the sampling took place at a moment of decline of the spring bloom (Fig. 4e); with the maximum occurring at the end of October–beginning of November (Fig. 4a, b, c). In the summer period, the maximum value of $Chla_{sat}$ was 8.78 mg m^{-3} and the minimum was 0.49 mg m^{-3}, both located in the external region of the gulf (>64°W, Fig. 4l). Overall the $Chla_{sat}$ in summer was decreased in comparison with the spring (Fig. 4), however, high values were maintained in the frontal zones and in the NL, and after the summer cruise an increase in the central region of the gulf and in the external zone was observed (Fig. 4m, n, o, p).

A time series of weekly values of $Chla_{sat}$ for sites selected to describe conditions across the SJG (corresponding to the positions I: st. 226 in the south, II: st. 211 in the center and III: st. 280 in the north, according to station numbers in the spring cruise) showed clearly that the spring sampling was done after the peak of the bloom (Fig. 5). Site I still had higher $Chla_{sat}$ values than the other sites during the spring cruise, and showed a similar value during the summer cruise (corresponding to st. 51), and also seemingly another peak during autumn; while $Chla_{sat}$ at sites II and III remained at relatively low values (Fig. 5).

To assess differences in the environmental conditions on the coasts and center of the gulf (Fig. 6a), a plot show-

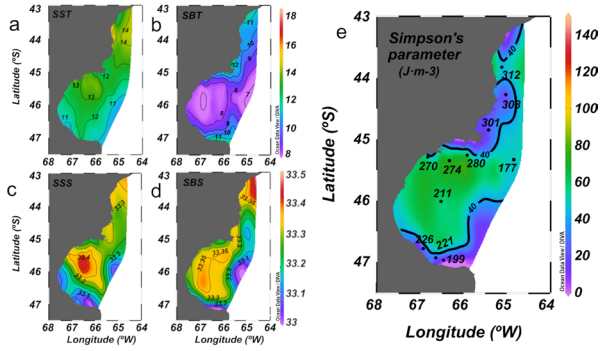

Fig. 2. Distribution of the temperature (**a**) at the surface, (**b**) at the bottom; and distribution of the salinity (**c**) at the surface and (**d**) at the bottom. A plot of the Simpson's parameter identifying the location of the frontal regions is shown (**e**) for spring (*PP* stations are marked).

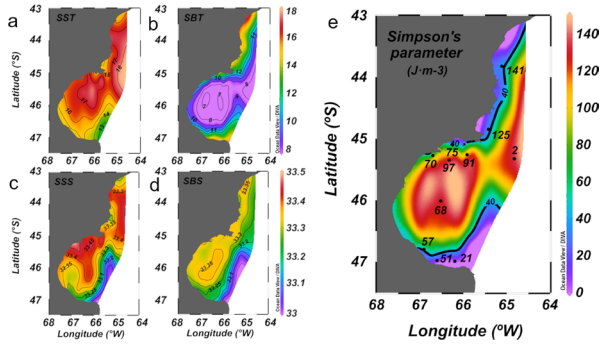

Fig. 3. Distribution of the temperature (**a**) at the surface, (**b**) at the bottom; and distribution of the salinity (**c**) at the surface and (**d**) at the bottom. A plot of the Simpson's parameter identifying the location of the frontal regions is shown (**e**) for summer (*PP* stations are marked).

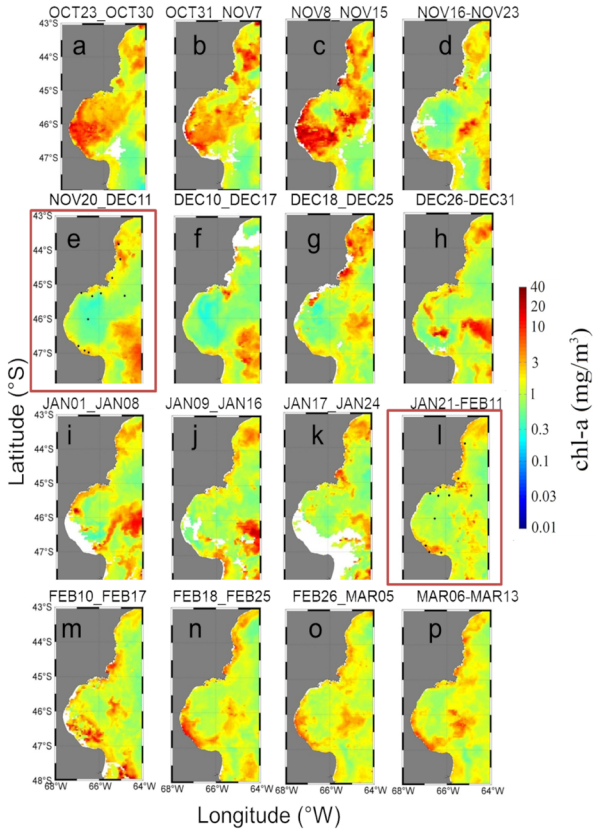

Fig. 4. Succession of weekly satellite images of $Chla_{sat}$ (mg m^{-3}) from Aqua-MODIS L3 SMI, (**a, b, c, d**) previous, (**e**) during and (**f, g, h**) after the spring cruise, (**i, j, k**) previous, (**l**) during and (**m, n, o, p**) after the summer cruise. Black circle symbols indicate *PP* stations.

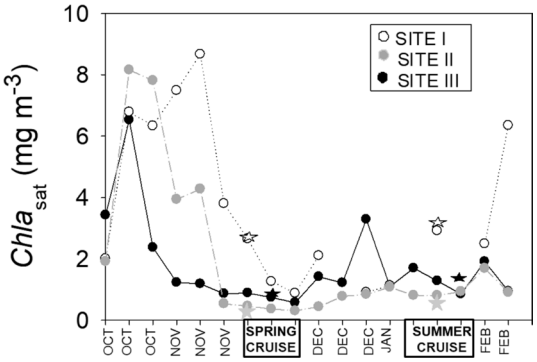

Fig. 5. Time series of values of weekly Cha_{sat} for selected sites: I (south), II (center) and III (north), located in a section across the SJG. The star symbols indicate when *in situ* samples were collected.

ing vertical variations in temperature, salinity and fluorescence across the area (South to North) was drawn (Fig. 6b, c and d). The thermocline appeared less pronounced and shallower on the southern coast, where it reached the surface leaving a homogeneous coastal zone; and then it intensified and got deeper to the center and north of the section (Fig. 6b). The salinity profile clearly showed low

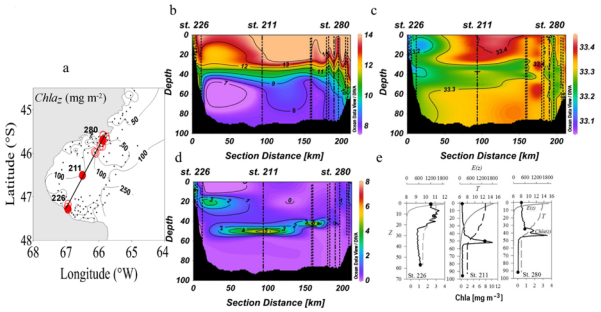

Fig. 6. Section across the SJG including the stations 226, 211 and 280 (**a**) Distribution of isolines of $Chla_Z$ in the area. Distribution of the gradients for the spring cruise of: (**b**) temperature, (**c**) salinity and (**d**) fluorescence. Vertical profiles (**e**) of: temperature (*T*), downwelling irradiance (*Ez*) and chlorophyll a (*Chla*) for the selected stations.

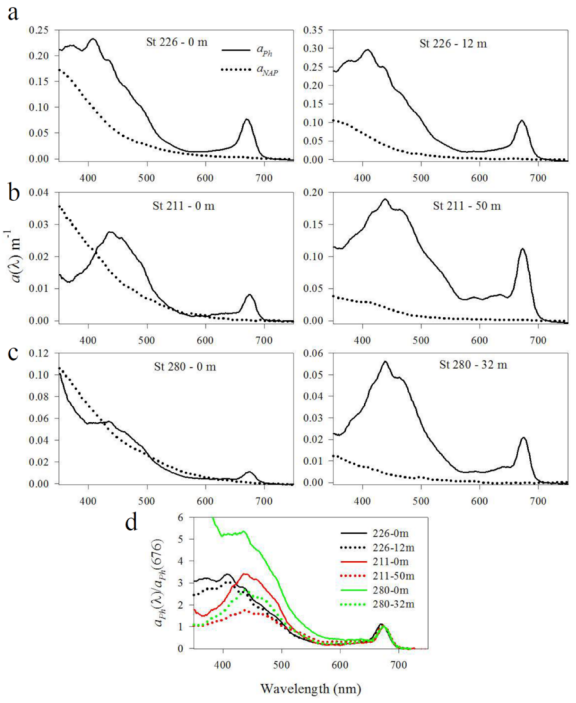

Fig. 7. Spectral absorption of phytoplankton (a_{ph}) and non-algal particles (a_{NAP}) for stations (**a**) 226, (**b**) 211 and (**c**) 280 at the surface and second sampled depth. Spectral absorption normalized at 676 nm for the three selected stations (**d**).

salinity waters in the south and (a milder signal) in the north, throughout most of the water column, indicating the entrance of waters from a branch of Patagonian Current, and higher values at the center especially in the upper layer (Fig. 6c). The fluorescence values showed a deepening of the signal from near the surface at the south to about 50 m at the center with a slight shoaling towards the northern coast, following the thermocline distribution (Fig. 6d). These features can be observed in detail in the individual profiles of stations 226 (southern coast), 211 (center), and 280 (northern coast), where a sharp deep chlorophyll maximum (*DCM*) is evident at the center (Fig. 6e). It can be

observed that the E_Z at the coastal stations is extinguished (E_z<1% E_s) at a shallower depth (around 16 m at st. 226, and 39 m at st. 280), and it reaches up to about 90 m at the center (Fig. 6e). This is probably due to the heavy load of suspended matter, as shown by the $a_{NAP}(440)$ for surface samples at stations 226 and 280 being about 4 times higher than at station 211 (Fig. 7) . The absorption spectra of phytoplankton and non-algal-particles for these three stations is evidence that NAP was always higher at the surface than at the second depth, bearing in mind that this second depth was not too close to the bottom, and this could be due to the intense westerly winds prevalent in the area bringing dust from the arid Patagonian landscape (Fig. 7). Phytoplankton absorption showed variations in spectral shapes, $a_{ph}(\lambda)/a_{ph}(676)$, indicating the presence of different taxonomic groups or different physiological states at the different stations of the section (Fig. 7d). It is clear for stations 211 and 280 that surface samples had higher values of $a_{ph}(440)/a_{ph}(676)$ than those from the second depth, which is expected in cells acclimated to higher light conditions (Sosik & Mitchell 1995), that was less marked at station 226 since the water column was well mixed and the second depth was not far from the surface (12 m). At this last station (226) another noticeable feature is that although there is a shoulder around 440 nm (usual peak in healthy phytoplankton), the maximum value was shifted towards 410 nm wavelength at which degradation products of chlorophyll absorb (Babin et al. 2003). This could have been due to senescent cells being removed from the bottom at this well-mixed coastal site (station depth ~60 m); on the other hand, during microscope analysis not many cells were in bad condition (broken or collapsed). Hence, another factor that could have contributed to this absorption spectral shape may be because the dominant diatom species was *Asteronellopsis glacialis* (Castracane) which is known to be highly susceptible to the decomposition of chlorophyll into chlorophyllide (easily converted into phaeophorbide absorbing at 410 nm) under the stress of filtration (Jeffrey & Hallegraeff 1987).

Variability in the photosynthetic and bio-optical properties

High variations in photosynthetic and bio-optical properties were observed in the two periods (Table 2). *Chla* at the stations where primary production experiments were performed ($Chla_{sPP}$) showed similar ranges in spring (0.32 to 2.38 mg m^{-3}) and in summer (0.54 to 2.63 mg m^{-3}). The total range of variation for the phytoplankton specific absorption coefficient $a^B_{ph}(440)$ at the surface was from 0.027 to 0.124 m^{-2} (mg *Chla*)$^{-1}$ (Table 2). The variability in the parameters P^B_m and α^B in both periods was over one order of magnitude, P^B_m ranged from 0.97 to 10.08 mg C (mg *Chla*)$^{-1}$ h^{-1} and α^B from 0.027 to 0.206 mg C (mg *Chla*)$^{-1}$ h^{-1} (W m^{-2})$^{-1}$. The lowest value of P^B_m was found in summer at st. 21, associated with low values of p_0 (p_0=0.797 mg C m^{-3} h^{-1}). Overall Φ_m had similar means and ranges for both periods (Table 2). Φ_m was higher where there was more phytoplankton and higher integrated production; i.e., where phytoplankton was growing under favorable conditions such as the SPSF in spring (st. 226 had one of the highest values of Φ_m 0.0134 mol C mol quanta^{-1}).

During spring 2008, *in situ Chla* values for the whole area and all sampled depths (including stations where no *PP* was estimated) ranged from 0.23 mg m^{-3} (st. 246 at 0 m) to 8.80 mg m^{-3} (st. 185 at 46 m). There was a marked vertical variation in *Chla* distribution: a) at the surface values were low (except at the southeast coast and up to the NL), b) in intermediate layers a *DCM* was evident with *Chla* values >8 mgm^{-3} at the center and in the south in the external zone, and c) at depths closer to the bottom *Chla* concentrations decreased extremely (except at the SPFS which was well mixed) (data not shown). The spatial distribution of the photosynthetic parameters showed the maximum values associated with the maximum values of p_0 were obtained at st. 226 (p_0=24.047 mg C m^{-3} h^{-1}). During this spring, high values of $Chla_z$ were observed in the area (Fig. 6a); specially values of $Chla_{ZPP}$>60.0 mg m^{-2} were located in the south and center of the gulf and adjacent waters (Fig. 6a), related to high primary production values.

During summer 2009, *in situ Chla* ranged from 0.09 mg m^{-3} (st. 79 at 0 m) to 5.31 mg m^{-3} (st. 7 at 40 m). The distribution of *Chla* in this period was spatially more homogeneous and lower than in spring at all sampled depths, with slightly higher values in the southern region at the surface (Cape Dos Bahías) and in the external zone, especially at the second sampled depth (data not shown).

Table 2. Ranges of variation in the photosynthetic and bio-optical properties for spring (2008) and summer (2009) at SJG.

Properties	spring range	mean	summer range	mean	Total range	mean
α^B	0.027–0.206	0.085	0.040–0.129	0.083	0.027–0.206	0.084
P^B_m	1.420–10.080	4.931	0.973–8.280	4.294	0.973–10.080	4.613
p_0	0.430–24.047	6.83	0.797–9.514	4.93	0.430–24.047	5.88
$P_{Z,T}$	813–3,523	1702	173–926	521	173–3,523	1,112
Φ_m	0.003–0.013	0.007	0.003–0.014	0.008	0.003–0.014	0.007
$Chla_{sPP}$	0.32–2.38	1.17	0.54–2.63	1.19	0.32–2.63	1.18
$a^B_{ph}(440)$	0.029–0.124	0.068	0.027–0.088	0.060	0.027–0.124	0.064

Integrated water column primary production

Values of integrated water column primary production ($P_{Z,T}$) were also highly variable in both periods (Fig. 8). In spring, the mean value of $P_{Z,T}$ (1702 mg C m^{-2} d^{-1}) was three times higher than in summer (521 mg C m^{-2} d^{-1}) (Table 2, Fig. 8). Overall, in summer the $P_{Z,T}$ values were not high, except at st.125 (Fig. 8).

Phyto- and Protozoo-plankton communities at the surface

During spring 2008 the distribution of total phytoplankton biomass (B_C) showed high values in the south of the gulf, including the maximum (89.2 mg C m^{-3} at st. 226) and in the adjacent shelf waters (st. 177) and the NL at st. 312 (Fig. 9). The dominant size fractions were the *Nano* and *Micro*, composed mainly of diatoms and dinoflagellates and in less proportion, by cryptophytes, prasinophytes and euglenophytes (Table 3). During this spring, two maxima of diatom biomass were observed: one at st. 226, located in the south of the gulf (51.5 mg C m^{-3}), dominated by *Asterionellopsis glacialis* (*Nano*); and the other at st. 177, located in the adjacent shelf waters (20.6 mg C m^{-3}), dominated by *Corethron criophilum* (Castracane) (*Micro*). The bloom at st. 226, although dominated by diatoms, also had a high contribution to the total biomass by the dinoflagellate *Heterocapsa* sp. (Stein) (*Nano*) (19.8 mg C m^{-3}) (Table 3). Another isolated maximum due to the dinoflagellate *Prorocentrum micans* (Ehrenberg) (*Nano*) was observed at st. 312 in the NL. The total protozooplankton biomass showed the highest values in the NL (st. 308 ~33.3 mg C m^{-3}) and along the southern coast of the SJG (st. 226 ~20.0 mg C m^{-3}). Heterotrophic dinoflagellates belonging to *Gyrodinium sp* (Kofoid & Swezy) and unknown naked ciliates of the *Micro* fraction dominated the protozooplankton biomass (Table 3).

During summer 2009, the maximum B_C, with a value of 45.8 mg C m^{-3}, was found at st. 51 in the south of the gulf, and was lower compared to the maximum found in spring (Fig. 10 and Table 4). However, in the north (B_C ~30.0 mg C m^{-3}) and in the center (B_C ~28.6 mg C m^{-3}) region of the gulf, higher values of *Bc* were observed in summer compared to spring (Fig. 10). The *Ultra* fraction represented the larger contribution to the total biomass and was dominated by *Synechococcus* sp. (stations. 51, 57, 68 and 70), while the *Nano* fraction represented a minor proportion of the total, and was composed mainly of dinoflagellates, cryptophytes and diatoms (Table 4). The *Micro* fraction contributed significantly to the total biomass only at two stations (Fig. 10, composed mainly of *Leptocylindrus danicus* (Cleve) (st. 51) and the phototrophic ciliate *Mesodinium rubrum* (Leegaard) (st. 75). In this period, the total protozooplankton biomass had high values with a maximum of 34.3 mg C m^{-3} at st. 51. On the whole, microplanktonic naked ciliates of the genus *Strombidium* dominated the protozooplankton biomass, with a special case

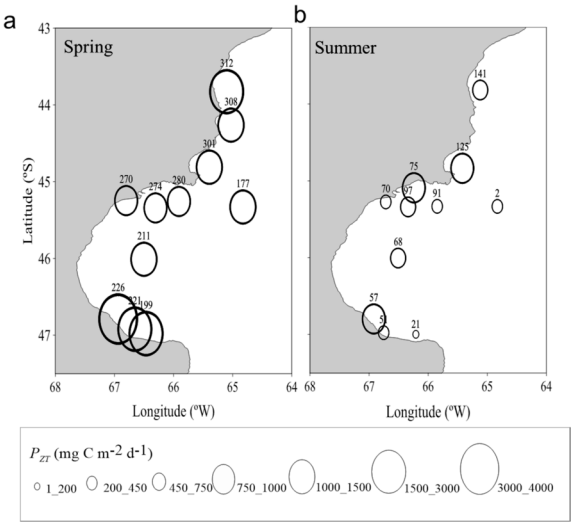

Fig. 8. Distribution of water column integrated primary production in (**a**) spring 2008 and (**b**) summer 2009.

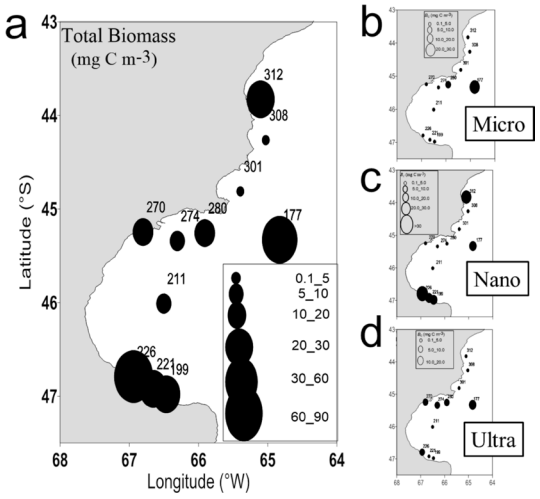

Fig. 9. Spatial distribution of surface phytoplankton biomass in terms of carbon during spring 2008 (**a**) for the whole community and for (**b**) Micro, (**c**) Nano and (**d**) Ultra size fractions. Note that the scales are different for each plot.

at station 51, where it was mostly composed of unknown ciliates of 100 μm diameter (Table 4).

Higher values of H' were registered in spring (H'>1.45) in comparison to summer (H'<0.58), except for station 21 in summer, where the maximum of H' was observed with a value of 2.37. A significant *Spearman* correlation (r_s) was found between H' and B_C (r_s=−0.049, p<0.05), but no significant relationship was observed between H' and p_0.

Discussion

The SJG and the NL showed, during the two periods studied, highly heterogeneous characteristics in photosynthetic and bio-optical properties in relation to the plank-

Table 3. Biomass (mg C m^{-3}) of identified phyto- and protozoo-plankton assemblages sorted by size fraction for the different stations sampled in spring 2008 at SJG.

Size	Type	Class/Group	Taxa	177	199	211	221	226	270	274	280	301	308	312
Microplankton 20–200 μm	Phyto	Bacillariophyceae	*Corethron criophilum*	20.6										
		Dinophyceae	*Alexandrium tamarense*		0.2		1.1	6.6	0.05		<0.1		0.1	
			Neoceratium lineatum	1.6	0.2	1.6	<0.1	0.1	1.2	2.5	4.8	0.2		<0.1
			Torodinium robustum	0.9		0.1	0.3	0.3	0.2	0.03	0.3	0.2		
		Euglenophyceae	*Eutreptiella* sp.		1.5		<0.1	0.4					0.1	2.2
		Total Micro Phyto		**23.1**	**1.9**	**1.7**	**1.4**	**7.4**	**1.5**	**2.5**	**5.1**	**0.4**	**0.2**	**2.2**
	Proto	Litostomatea	*Mesodinium rubrum*	0.3	0.8		1.3	0.9		1.1	0.4	0.1	0.8	
		Naked Cilliates	Oligotrichia	0.9	6.6	0.3	5.4	1.2	11.5	3.0	10.3	15.6	30.4	16.7
		Dinophyceae	Mainly *Gyrodinium* sp.	1.9	6.7	0.4	2.9	18.2	7.1	0.7	4.8	1.6	0.1	0.1
		Total Micro Proto		**3.1**	**14.1**	**0.7**	**9.6**	**20.3**	**18.6**	**4.8**	**15.5**	**17.3**	**31.3**	**16.8**
Nanoplankton 5–20 μm	Phyto	Bacillariophyceae	*Asterionellopsis glacialis*		13.5		6.0	51.5						<0.1
			Guinardia sp.	1.9										
			Hemiaulus sp.	12.6										
		Cryptophyceae	Cryptophytes	0.3	0.7	<0.1	1.5	2.3	<0.1			0.7	0.3	
		Dinophyceae	*Scrippsiella* sp.	0.3	1.6		8.5	0.9	0.2					
			Gymnodiniales				2.7							
			Heterocapsa sp.					19.8		0.1	0.5	0.4		0.7
			Prorocentrum micans	0.9		<0.1	<0.1		<0.1	0.1	0.1	0.1	<0.1	16.4
		Total Nano Phyto		**16**	**15.8**	**0.05**	**18.7**	**74.5**	**0.2**	**0.2**	**0.6**	**1.2**	**0.3**	**17.1**
	Proto	Dinophyceae	Gymnodiniales	1.0	0.5	0.9	2.0	0.2	0.7	0.1	<0.1		<0.1	1.3
		Heterotrophic flagellates	Unknown flagellates	0.8	0.2	2.9			1.3	1.1				1.3
		Total Nano Proto		**1.8**	**0.7**	**3.8**	**2**	**0.2**	**2**	**1.2**	**<0.1**		**<0.1**	**1.6**
Ultraplankton 0.2–5 μm	Phyto	Prymnesiophyceae	*Emiliania huxleyi*			0.03							0.1	3.8
		Prasinophyceae	*Pyramimonas* sp.	0.2	2.7		1.9	1.3	0.2	0.1		0.4	0.2	0.2
		Unidentified cells	Picophytoeukaryotes		0.4		0.4	4.8						
		Cyanobacteria	*Synechococcus* sp.	16.3	0.5	4.6	1.6	1.2	8.4	5.6	6.5			
		Total Ultra Phyto		**16.5**	**3.6**	**4.6**	**3.9**	**7.3**	**8.6**	**5.7**	**6.5**	**0.4**	**0.3**	**4**
	Proto	Ultraprotozooplankton		2.1		2.2	1.1	0.5	0.9	1.1	2.7	1.3	1.7	2.3
		Total Ulta Proto		**2.1**		**2.2**	**1.1**	**0.5**	**0.9**	**1.1**	**2.7**	**1.3**	**1.7**	**2.3**
		Total Phyto		**55.6**	**21.3**	**6.35**	**24**	**89.2**	**11.6**	**8.4**	**12.2**	**2.0**	**0.8**	**23.3**
		Total Proto		**7.0**	**14.8**	**6.7**	**15.5**	**21.0**	**21.5**	**7.1**	**17.3**	**18.6**	**33.3**	**20.7**

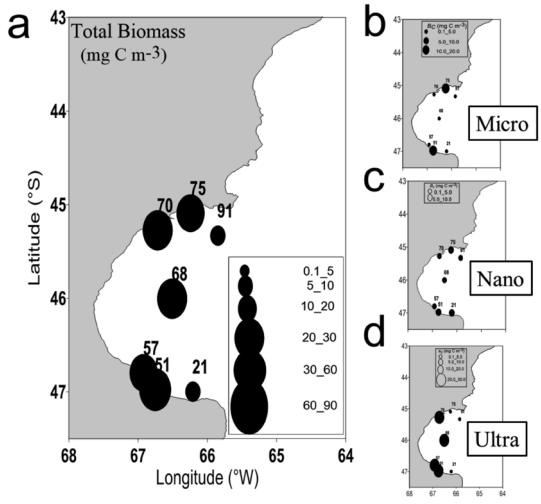

Fig. 10. Spatial distribution of surface phytoplankton biomass in terms of carbon during summer 2009 (**a**) for the whole community and for (**b**) Micro, (**c**) Nano and (**d**) Ultra size fractions.

ton assemblages present and to the physical environment, which resulted in a large fluctuation in the primary production. This biological and physiological variability is not uncommon for the region; a high level of heterogeneity has already been reported from extensive cruises in the Argentine Sea (Segura et al. 2013). The maximum integrated production found along the south coast of the SJG in spring ($P_{Z,T}$=3,500 mg C m^{-2} d^{-1}) was in the range previously observed also in spring in regions considered within the most productive in the world ocean, such as the shelf break front (Garcia et al. 2008, Lutz et al. 2010, Segura et al. 2013) and the coastal front of Grande Bay and the Puerto Deseado region (Lutz et al. 2010, Segura et al. 2013); which are also important fishing grounds mainly for squid and hoki (Brunetti et al. 1998, Giussi et al. 2016). Overall $\varnothing_m$ had similar means and ranges for both periods (Table 2) and had relatively low values in the SJG, comparable to those found in the oligotrophic northeast Atlantic ($\varnothing_m$=0.005–0.063 mol C mol quanta^{-1}; Babin et al.

Table 4. Biomass (mg C m^{-3}) of identified phyto and protozoo-plankton groups sorted by size fraction for the different stations sampled in summer 2009 at SJG.

Size	Type	Class/Group	Taxa	21	51	57	68	70	75	91
Microplankton 20–200 μm	Phyto	Bacillariophyceae	*Leptocylindrus danicus*		17.8	0.2			1.7	
		Dinophyceae	*Alexandrium catenella*						0.9	<0.1
			Ceratium lineatum	0.2			0.3	0.1	1.0	0.2
			Torodinium robustum	0.1		0.1	1.2	0.2	0.1	0.2
		Total Micro Phyto		**0.3**	**17.8**	**0.3**	**1.5**	**0.3**	**3.7**	**0.4**
	Proto	Litostomatea	*Mesodinium rubrum*		0.3		0.1		9.8	
		Naked Cilliates	Oligotrichia	2.9	30.5	2.9	22.4	12.5	16.4	13.8
		Dinophyceae	Mainly *Gyrodinium* sp.		1.0	<0.1	0.1		0.8	<0.1
		Total Micro Proto		**2.9**	**31.8**	**2.9**	**22.6**	**12.5**	**27**	**13.8**
Nanoplankton 5–20 μm	Phyto	Bacillariophyceae	*Asterionellopsis glacialis*						0.1	
			Rhizosolenia sp.						5.6	
		Cryptophyceae	Cryptophytes		6.1			0.9	0.2	
		Dinophyceae	*Heterocapsa* sp.	<0.1			1.2	0.1		
			Gymnodiniales	4.9						
			Prorocentrum micans	1.7	<0.1		0.2	0.1	1.2	3.0
			Scrippsiella sp.						1.7	
		Prymnesiophyceae	*Braarudosphaera bigelowi*				0.3	0.1	<0.1	0.7
			Emiliania huxleyi	1.1	0.1	0.1	0.6	0.3	<0.1	0.1
		Total Nano Phyto		**7.7**	**6.2**	**0.1**	**2.3**	**1.5**	**8.8**	**3.8**
	Proto	Naked Cilliates	Oligotrichia	1.5				0.6		0.3
		Dinophyceae	Gymnodiniales	2.7	0.8	0.3		0.5	0.4	2.0
		Katablepharidaceae	*Leucocryptos* sp.	1.4	0.2	0.6	0.2	0.8	0.4	0.4
		Telonemia	*Telonema* sp.			0.5		1.1	0.2	
		Total Nano Proto		**5.6**	**1**	**1.4**	**0.2**	**3**	**1**	**2.7**
Ultraplankton 0.2–5 μm	Phyto	Cryptophyceae	Cryptophytes		1.4		0.1	0.6		
		Cyanobacteria	*Synechococcus* sp.		18.7	25.5	24.6	26.5	2.9	3.5
		Prasinophyceae	*Pyramimonas* sp.		1.3	0.6	<0.1	0.2	0.1	
		Prymnesiophyceae	*Chrysochromulina* spp.	<0.1	0.4	0.6	0.1	0.9	<0.1	0.2
		Total Ultra Phyto		**0.02**	**21.8**	**26.7**	**24.8**	**28.2**	**3**	**3.7**
	Proto	**Total Ultra Proto**		**1.7**	**1.5**	**0.5**	**0.9**	**0.6**	**0.4**	**0.5**
		Total Phyto		**8.0**	**45.8**	**27.1**	**28.6**	**30.0**	**15.5**	**7.9**
		Total Proto		**10.2**	**34.3**	**4.8**	**23.7**	**16.1**	**28.4**	**17.0**

1996). Values of $Ø_m$ are extremely variable in nature (due to changes in species, light and nutrient regimes); one of the contributing factors to the low yields found for the SJG could be that in the present study estimations were done only at the surface and $Ø_m$ is known to increase with depth (Kirk 2011).

Biodiversity is an indicator of the health of an ecosystem; the SJG is being disturbed by anthropogenic actions and the resilience of this system would depend to a great part on its degree of biodiversity. Here the rank of values estimated for the Shannon diversity index of phytoplankton, 0.06–2.37 bits individual^{-1}, is comparable to those found in other coastal environments (Estrada et al. 2004). High diversity is usually associated with permanent stocks of high biomass in terrestrial ecosystems, while the opposite is common in marine ecosystems, where an increase in production has been reported to be associated with a decrease in diversity (Pearl 1988). On the other hand, in the SJG high diversity values were found during spring, coinciding with high primary production; so far there are no obvious explanations for our results.

Previous studies have reported that the annual cycle of phytoplankton biomass in the SJG is typical of temperate seas with two maxima, one in spring and the other, of lower magnitude, in autumn (Akselman 1996, Cuchi Colleoni & Carreto 2000, Fabro et al. 2018). Consequently, *Chla* and B_C values observed here exhibited a maximum during spring and a decrease in summer; the same pattern was observed for primary production. The phytoplankton biomass (in carbon) was dominated by the *Nano* and *Micro* fractions in spring and by the *Ultra* for the summer period, with a high contribution of *Synechococcus* sp. The *Chla* in the summer period although relatively lower than in spring, maintained high values at the frontal regions, as observed previously (Rivas et al. 2006, Carreto et al. 2007).

During 2008, the spring bloom was evident in the southern coastal sector of the gulf (especially st. 226) and was mainly produced by the diatom *Asterionellopsis glacialis* and the dinoflagellate *Heterocapsa* sp., both species characteristic of turbulent environments (Lindholm & Nummelin 1999, Odebrecht et al. 2010), as was the case at this station, where the water column was fairly homogeneous (Fig. 6e). Although, according to the sequence of satellite images, the bloom was already in decline (Fig. 5), microscopic examination of the cells showed that the cell membrane and cytoplasm content, especially the plastids, were in good condition, indicating that the cells were healthy. At station 226, phytoplankton biomass was the highest (B_C ~85 mg C m^{-3}), coincident with the maximum value of p_0 (24.047 mg C m^{-3} h^{-1}), and also the maximum values for this study of the photosynthetic parameter P_m^B (10.080 mg C (mg *Chla*)$^{-1}$ h^{-1}). Here the apparent productivity yield per unit carbon biomass was higher than that found during spring 2005 (Segura et al. 2013) at a high productivity spot in Grande Bay (produced by a bloom of the dinoflagellate *Prorocentrum minimum* (Pavillard-Schiller), also belonging to the *Nano* size fraction), where *Bc* was ~350 mg C m^{-3} (Goméz et al. 2011) and p_0=39.63 mg C m^{-3} h^{-1} (Lutz et al. 2010). This difference could be due to the different phytoplankton species and to modulation of the photosynthetic parameters, especially P_m^B which was ~30% higher (st. 226, 2008) than that in spring 2005, to acclimate to the light and nutrient environment to which the cells were exposed. Here, incident irradiance was three-fold higher at st. 226 (2008) than at the site of the Grande Bay bloom in 2005, indicating that light was probably the determining driver of production.

Vertical sections of temperature, salinity and fluorescence drawn for a selected section in spring (Fig. 6b, c and d) showed the entry of a cold and low salinity water mass coming from the south. Particularly, the southern stations (st. 226, st. 227 and st. 228) were mixed, while the central region of the SJG (st. 211) showed a stratified water column in the upper 60 meters, with high salinity values and a maximum of fluorescence at the base of the stratified layer. The northern region showed low stratification, intermediate salinity values and low fluorescence. The special situation developed at the center (st. 211) was observed also in the biological characteristics, where the value of P_{ZT} was relatively low in comparison with the high value of $Chla_Z$. This was because a large *DCM* was found at ~50 m, where light was already strongly attenuated (Fig. 6e), even when phytoplankton was apparently still active at this depth, based on to the *Chla* concentration and the shape of the absorption spectrum (Fig. 7b). At this station, *Synechococcus* was a main component of the phytoplankton at the surface, though unfortunately no information was available for the *DCM*. Different factors, or a combination of them, can produce conspicuous *DCMs* (Cullen 2015). We can speculate that this high chlorophyll concentration at depth at station 211 could have been due to: a) the growth of the same population of ultra-phytoplankton present at the surface but acclimated to low light; b) preferential aggregation by motile phytoplankton (e.g., dinoflagellates), considering that the station was sampled at night; c) larger cells that have sunk after nutrients were depleted in the upper layer due to the peak of the previous bloom that was observed at the surface in the satellite images (Figs. 4a and 5). The latter seems a plausible hypothesis, and since the absorption spectrum was the same as that of healthy cells it would indicate that either they had very recently precipitated or that part of the population acclimated to the relatively low light (increasing the intracellular concentration of *Chla*; hence emphasizing the *DCM* effect) and probably received nutrients by some degree of exchange across the thermocline. Moreover, Palma et al. (2020) have recently modelled the effect of geostrophic circulation in the intermediate layer in this zone of the SJG that generates a cyclonic gyre (Fig. 1), which could favor the retention of this high phytoplankton biomass (*Chla*) encountered at the *DCM*. This phytoplankton located at depth would most probably precipitate to the bottom, which is consistent with the reported presence of fine sediments in this central region of the gulf characterized by high amounts of total organic matter (Fernández et al. 2005, Kamisky et al. 2018). This spot is also an example where satellite surface estimates of *Chla* would not represent well the richness of phytoplankton biomass at the site once a *DCM* is established.

A positive relationship between the rate of primary production and *Chla* at the surface and carbon biomass was clear for spring, though a high dispersion of the data was observed for summer (data not shown). This variability in summer could be due to the different communities present and their varying physiological state. For example at st. 75, dominated by *Mesodinium rubrum* (a protozooplankton with cryptophyte symbionts) in the *Micro* fraction, a high *PP* was coincident with a high *Bc*; while at st. 51, dominated by the diatom *Leptocylindrus danicus,* also in the *Micro* fraction, a low *PP* was found although *Bc* was relatively high, but these cells, observed under the microscope, showed broken or collapsed plastids indicative of poor health conditions.

Phytoplankton biomass (B_C) is an important source of organic carbon in the flow of matter through the pelagic food web (Legendre & Rassoulzadegan 1995) and contributes to the sedimentation processes towards the benthos (Smetacek 1985, Legendre 1990). It was observed here that, during spring, part of the organic carbon produced in the southern region of the SGJ would be channeled by the protozooplankton component, especially heterotrophic dinoflagellates, which are known to be a main trophic nexus between phytoplankton and the upper trophic levels (Sherr & Sherr 2007, 2009); which in turn can be eaten by shrimp larvae. Another part of the organic carbon produced at the frontal area in the south of the SJG could be fueled to the benthos, the community of which is dominated by filter feeders (Giberto et al. 2015, Kaminsky et al.

2015). Contrary to this, during summer a microbial food web developed, fueled by ultraphytoplankton as a carbon source, as has been observed in other studies (Williams et al. 2018, Flores Melo et al. 2018). At this time of the year, a lower and more homogeneous spatial distribution in B_C was observed inside the SJG, marked by the dominance of small sized cells, mainly *Synechococcus* sp, where the main predators were naked ciliates. Only at the frontal zones was the phytoplankton biomass high in summer, and this was due to the presence of a few large sized individuals such as the diatom *Leptocylindrus danicus*, in the SPFS front and the photosynthetic ciliate *Mesodinium rubrum* in the NPFS front, which due to their weight are more susceptible to sinking and contribute to benthic and multivorous trophic webs (Legendre & Rassoulzadegan 1995).

In the present study we found that in the two frontal zones (NPFS and SPFS) a high chlorophyll *a* was related to high carbon biomass and high phytoplankton productivity in spring, and this high *Chla* remained relatively high even in summer. In concordance, in these frontal zones high abundances of impregnated female shrimps, as well as eggs and larvae, have been observed in spring and summer (Fernández et al. 2012). In the 2009 cruise, eggs and larvae were found throughout the study area and the highest concentrations of eggs were detected in the south of the gulf and NL in Escondida island (Moriondo Danovaro 2010). The presence of protozoea and mysids, in summer 2009, in relatively high densities compared to previous years indicates that a large proportion of the eggs that were spawned in the spring of 2008 survived until reaching the most advanced larval stages (Moriondo Danovaro 2010).

The high phytoplankton biomass and productivity would have contributed to a large amount of organic matter sinking to the bottom, which would provide good nutrition for impregnated female shrimp; since it has been reported that these shrimp have a detritivorous feeding habit. Even more, the permanence of relatively high phytoplankton biomass in these areas during summer, and especially its increase in autumn, would favor the feeding of shrimp larvae on pelagic biomass. Hence, there is evidence that high primary production found at SJG supports food webs, which includes the main fisheries targets of the shrimp *Pleoticus muelleri* (Bate, 1888), the hake *Merluccius hubbsi* (Marini, 1933) and the southern king crab *Lithodes santolla* (Molina, 1782).

Concluding Remarks

The occurrence of different plankton (phyto and protozoo) types found here indicated differences in the structure of the food webs in the SJG between spring and summer. Variations found in the structure and physiology of plankton affects the pelagic and benthic communities, including the life cycles of the most important fishing species in the area like shrimp. It was clear that frontal zones in the north and south of the gulf, favoring high phytoplankton B_C and its maintenance due to a high *PP*, provided a favorable food environment for the impregnated female shrimp in spring and that of larvae during summer. Another important ecological function that became apparent in the central part of the gulf was the presence of a *DCM,* which would indicate an active biological pump that contributes to sedimentation of organic matter to the bottom.

To further understand the functioning of the San Jorge Gulf ecosystem, and how susceptible it could be to changes in the environment, it is necessary to extend these plankton and primary production studies to cover the whole annual cycle and to continue the inter-annual monitoring during spring-summer (when plankton and larvae are abundant) to assess possible changes related to natural or anthropogenic (climate change) causes.

Acknowledgements

This work was financed by INIDEP, and partially by CONICET (MLC and VL). Contributions received by colleagues from INIDEP, especially C. Berghoff, A. Baldoni, D. Cuchi Colleoni, D Hernández and M. Fernández, are greatly appreciated. We would like to thank the crew of the R/V Capitán Oca Balda, as well as INIDEP authorities. This is INIDEP contribution 2226.

References

Akselman R (1996) Estudios ecológicos en el Golfo San Jorge y adyacencias (Atlántico sudoccidental). Distribución, abundancia y variación estacional del fitoplancton en relación a factores físico-químicos y a la dinámica hidrográfica. PhD Thesis, Universidad de Buenos Aires, Argentina, 234 pp.

Babin M, Morel A, Claustre H, Bricaud A, Kolber Z, Falkowski P (1996) Nitrogen- and irradiance dependent variations of the maximum quantum yield of carbon fixation in eutrophic, mesotrophic and oligotrophic marine systems. Deep-Sea Res 43: 1241–1272.

Babin M, Stramski D, Ferrari GM, Claustre H, Bricaud A, Obolensky G, Hoepffner N (2003) Variations in the light absorption coefficients of phytoplankton, non algal particles, and dissolved organic matter in coastal waters around Europe. J. Geophys. Res. 108: C7, 3211.

Bailey S, Werdell P (2006) A multi-sensor approach for the on orbit validation of ocean color satellite data products. Remote Sens Environ 102: 12–23.

Base Regional de Datos Oceanográficos (BaRDO), Instituto Nacional de Investigación y Desarrollo Pesquero: Gabinete de Oceanografía Física. Ministerio de Producción y Trabajo/ Agroindustria/Instituto Nacional de Investigación y Desarrollo Pesquero. Paseo Victoria Ocampo Nº1, Mar del Plata, Bs. As. Argentina. http://www.inidep.edu.ar/oceanografia/.

Bermejo P, Helbling EW, Durán-Romero C, Cabrerizo MJ, Villafañe VE (2018) Abiotic control of phytoplankton blooms in temperate coastal marine ecosystems: A case study in the South Atlantic Ocean. Sci Total Environ 612: 894–902.

Bertuche D, Fischbach C, Roux A, Fernández M, Piñero R

(2000) Langostino (*Pleoticus muelleri*). In: Síntesis del estado de las Pesquerías Marítimas Argentinas y de la Cuenca del Plata. Años 1997–1998, con la actualización de 1999 (eds Bezzi S, Akselman R, Boschi EE). INIDEP, Mar del Plata, Argentina, pp. 179–190.

Bezzi S, Verazay G, Dato C (1995) Biology and fisheries of Argentine hakes (*M. hubbsi* and *M. australis*). In: Hake: Biology, fisheries and markets (eds Alheit, Pitcher). Chapman and Hall, London, 478 pp.

Bianchi A, Masonneau M, Oliviera R (1982) Análisis estadístico de las características T-S del sector austral de la plataforma continental argentina. Acta Oceanogr Arg 3: 93–118.

Behrenfeld M, O'Malley RT, Sielgel DA, McClain C, Sarmiento JL, Feldman GC, Milligan AJ, Falkowski PG, Letelier RM, Boss E (2006) Climate-drivend trends in contemporary ocean productivity. Nature 444: 752–755.

Bogazzi E, Baldoni A, Rivas AL, Martos P, Reta R, Orensanz JM, Lasta M, Dell'Arciprete P, Werner F (2005) Spatial correspondence between areas of concentration of Patagonian Scallop (*Zygochlamys patagonica*) and frontal systems in the Southwestern Atlantic. Fish Oceanogr 14: 359–376.

Borsheim KY, Bratbak G (1987) Cell volume to cell carbon conversion factors for a bacterivorous *Monas* sp. enriched from seawater. Mar Ecol Prog Ser 36: 171–175.

Bouman HA, Platt T, Sathyendranath S, Stuart V (2005) Dependence of light-saturated photosynthesis on temperature and community structure. Deep Sea Res I 52: 1284–1299.

Bouman HA, Platt T, Doblin M, Figueiras FG, Gudmudsson K, Gudfinnsson HG, Huang B, Hickman A, Hiscock M, Jackson T, Lutz VA, Mélin F, Rey F, Pepin P, Segura V, Tilstone GH, van Dongen-Vogels V, Sathyendranath S (2018) Photosynthesis-irradiance parameters of marine phytoplankton: synthesis of a global data set, Earth Syst Sci Data 10: 251–266.

Brunetti NE, Ivanovic ML, Rossi GR, Elena B, Pineda SE (1998) Fishery biology and life history of *Illex argentinus*. In: Okutani T (ed.). Large Pelagic Squid. Japan Marine Fishery Resources Center (JAMARC) Special Publication. Tanaka Priniting Co. Ltd., Tokyo: 216–231.

Carreto J, Cucchi Colleoni D (2001) Variación estacional de la biomasa fitoplanctónica en el Golfo San Jorge. Resultados de las campañas de investigación: OB-01/00, OB-03/00, OB-10/00 y OB-12/00. Inf Téc Int INIDEP, 49: 30 pp.

Carreto JI, Carignan MO, Montoya NG, Colleoni DA (2007) Ecología del fitoplancton en los sistemas frontales del mar argentino. In: El mar Argentino y sus recursos pesqueros. Tomo 5, (eds Carreto JI, Bremec C), INIDEP, Mar del Plata, pp. 11–31.

Cuchi Colleoni DA, Carreto JI (2000) Variación estacional de la biomasa fitoplanctónica en el Golfo San Jorge. Resultados de las Campañas de Investigación OB-01/00, OB-03/00, 10/00 y OB-12/00. INIDEP Inf Téc Int 49: 30 pp.

Collos Y, Slawyk G (1985) On the compatibility of carbon uptake rates calculated from stable and radioactive isotope data: implications for the design of experimental protocols in aquatic primary productivity. J Plankton Res 7: 595–603.

Cullen J (2015) Subsurface chlorophyll maximum layers: Enduring enigma or mistery solved? Annu Rev Mar Sci 7: 207–239.

Cushing DH (1969) The regularity of the spawning season of some fishes. J Cons Int Explor Mer 33: 81–92.

Dans SL, Cefarelli AO, Galván DE, Góngora ME, Martos P & Varisco MA (eds.). (2020) Programa de Investigación y Monitoreo del Golfo San Jorge. Pampa Azul. Fundación de Historia Natural Félix de Azara. Buenos Aires. 99 pp.

Dogliotti AI, Lutz VA, Segura V (2014) Estimation of primary production in the southern Argentine continental shelf and shelf-break regions using field and remote sensing data. Remote Sens Environ 140: 497–508.

Dubinsky Z, Falkowski PG, Wyman K (1986) Light harvesting and utilization by phytoplankton. Plant Cell Physiol 27: 1335–1349.

El-Sayed SZ (1964) Productivity studies along the Argentine coast, Drake Passage and Weddell Sea. Texas, Texas A and M University. The Department of Oceanography and Meteorology, 45 pp.

El-Sayed SZ (1968) On the productivity of the Southwest Atlantic Ocean and the waters west of the Antartic Peninsula. In: Biology of the Antarctic Seas III. Antarctic Research Series 11 (eds Schmitt W, Llano GA). American Geophysical Society, Washington, pp. 15–47.

Estrada M, Henriksen P, Gasol JM, Casamayor EO, Pedrós-AlióC (2004). Diversity of planktonic photoautotrophic microorganisms along a salinity gradient as depicted by microscopy, flow cytometry, pigment analysis and DNA-based methods. FEMS Microbiol Ecol 49: 281–293.

Fabro E, Krock B, Torres A, Paparazzo F, Schloss I, Ferreyra G, Almandoz G (2018) Toxigenic Dinoflagellates and Associated Toxins in San Jorge Gulf, Argentina. Oceanography 31: 145–153.

Fernández C, Raimbault P, Garcia N, Rimmelin P (2005) An estimation of annual new production and carbon fluxes in the northeast Atlantic Ocean during 2001. J Geophys Res 110: doi: 10.1029/2004JC002616.

Fernández M, Mora J, Roux A, Fernández E, Caló J, Marcos A, Aldacur H (2003) Grain-size analysis of surficial bottom sediment samples from San Jorge Gulf. Argentine. J. Mar. Biol. Assoc. U.K. 83: 1193–1197.

Fernández M, Iorio MI, Hernández D, Macchi G (2012) Studies on the reproductive dynamics of *Pleoticus muelleri* (Spence Bate, 1888) (Crustacea, Decapoda, Solenoceridae) of Patagonia, Argentina. Latin American. J Aquat Res 40: 858–871.

Flores-Melo X, Schloss I, Chavanne C, Almandoz G, Latorre M, Ferreyra G (2018) Phytoplankton ecology during a spring-Neap Tidal Cycle in the Southern Tidal Front of San Jorge Gulf, Patagonia. Oceanography 31: 70–80.

Garcia VMT, Garcia CAE, Mata MM, Pollery RC, Piola A, Signorini SR, McClain C, Iglesias-Rodriguez MD (2008) Environmental factors controlling the phytoplankton blooms at the Patagonia shelf-break in spring. Deep-Sea Res I 55: 1150–1166.

Geider RJ, Platt T, Raven JA (1986) Size dependence of growth and photosynthesis in diatoms: a synthesis. Mar Ecol Prog Ser 30: 93–104.

Giberto DA, Romero S, Escolar MV, Machinandiarena L, Bremec C (2015) Diversidad de las comunidades bentónicas en las regiones de reclutamiento de la merluza común *Merluccius hubssi*, (Mariani 1933). Rev Invest Desarr Pesq 27: 5–25.

Giussi, A, Zavatteri A, Di Marco E, Gorini FL, Bernadele J, Marí NR (2016) Biology and fisheries of long tail hake from Atlantic Ocean (*Macruronus magellanicus*). Rev Invest Desarr Pesq 28: 55–82.

Glorioso PD (1987) Temperature distribution related to the shelf-sea fronts on the Patagonian Shelf. Cont Shelf Res. 7: 27–34.

Gregg WW, Casey NW, McClain C (2005) Recent trends in global ocean chlorophyll. Geophys Res Lett 32: L03606.

Goméz MI, Piola AR, Katiner G, Alder VA (2011) Biomass of autotrophic dinoflagellates under weak vertical stratification and contrasting chlorophyll levels in subantarctic shelf waters. J Plankton Res 33: 1304–1310.

Guerrero R, Piola A (1997) Masas de agua en la Plataforma Continental. In: El Mar Argentino y sus recursos pesqueros (ed Boschi EE). Tomo 1. INIDEP, Mar del Plata, Argentina, pp. 107–118.

Hama T, Miyazaki T, Ogawa Y, Iwakuma T, Takahashi M, Otsuki A, Ichimura S (1983) Measurement of photosynthetic production of a marine phytoplankton population using a stable ^{13}C isotope. Mar Biol 73: 31–36.

Hasle GR (1978) Using the inverted microscope. In: Phytoplankton manual. (ed Sournia, A.) UNESCO, 191–196.

Hillebrand H, Dürselen CD, Kirschtel D, Pollingher U, Zohary T (1999) Biovolume calculation for pelagic and benthic microalgae. J Phycol 35: 403–424.

Hoepffner N, Sathyendranath S (1992) Bio-optical characteristics of coastal waters: Absorption spectra of phytoplankton and pigment distribution in the western North Atlantic. Limnol Oceanogr 37: 1660–1679.

Holm-Hansen O, Lorenzen CJ, Holmes RW, Strickland DH (1965) Fluorometric determination of chlorophyll. J du Conseil 30: 3–15.

Jeffrey, SW, Hallegraeff GM (1987) Phytoplankton pigments, species and light climate in a complex warm-core eddy of the East Australian Current. Deep-Sea Res 34: 649–673.

Kaminsky J, Varisco M, Fernández M, Sahade R, Archambault P (2018) Spatial analysis of benthic functional biodiversity in San Jorge Gulf, Argentina. Oceanography 31: 104–112.

Kishino M, Takahashi M, Okami N, Ichimura S (1985) Estimation of the spectral absorption coefficients of phytoplankton in the sea. Bull Mar Sci 37(2): 634–642.

Kirk JT (2011) Light and photosynthesis in aquatic ecosystems. Third Edition. Cambridge, UK, Cambridge University Press, 649 pp. ISBN 978-0-521-15175-7.

Kovač Z, Platt T, Sathyendranath S, Lomas MW (2018) Extraction of photosynthesis parameters from Time Series Measurements of in situ production Bermuda Atlantic Time-Series Study. Remote Sens 10: 1–23.

Krock B, Borel CM, Barrera F, Tillmann U, Fabro E, Almandoz GO, Ferrario M, Garzón Cardona JE, Koch BP, Alonso C, Lara R (2015) Analysis of the hydrographic conditions and cyst beds in the San Jorge Gulf, Argentina, that favour dinoflagellate population development including toxigenic species and their toxins. J Mar Syst 148: 86–100.

Legendre L (1990) The significance of microalgal blooms for fisheries and for the export of particulate organic carbon in oceans. J Plankton Res 12: 681–699.

Legendre L, Rassoulzadegan F (1995) Plankton and nutrient dynamics in marine waters. Ophelia 41: 153–172.

Lindholm T, Nummelin C (1999) Red tide of the dinoflagellate *Heterocapsa triquetra* (Dinophyta) in a ferry-mixed coastal inlet. Hydrobiologia 393: 245–251.

Longhurst A, Sathyendranath S, Platt T, Caverhill C (1995) An estimate of global primary production in the ocean from satellite radiometer data. J Plankton Res 17: 1245–1271.

Lucas, AJ, Guerrero RA, Mianzan HW, Acha EM, Lasta CA (2005) Coastal oceanographic regimes of the Northern Argentine Continental Shelf (34–43°S). Est Coast Shelf Sc 65: 405–420.

Lutz VA, Segura V, Dogliotti AI, Gagliardini DA, Bianchi A, Balestrini CE (2010) Primary production in the Argentine Sea during spring estimated by field and satellite models. J Plankton Res 32: 181–195.

Lutz V, Frouin R, Negri R, Silva R, Pompeu M, Rudorff N, Cabral A, Dogliotti A, Martinez G (2016) Bio-optical characteristics along the Straits of Magallanes. Cont Shelf Res 119: 56–67.

Lutz V, Segura V, Dogliotti A, Tavano V, Brandini F, Calliari D, Ciotti AM, Villafañe V, Pompeu M, Schloss I, Saldanha Corrêa F, Benavides H, Vizziano Cantonnet D (2018) Overview on primary production in the Southwestern Atlantic. In: Plankton ecology of the Southwestern Atlantic. From the subtropical to the subantarctic realm. (eds Hoffmeyer M, Sabatini M, Brandini F, Calliari D, Santinelli N) Springer International Publishing, Switzerland, 586 pp.

Luz Clara M, Simionato CG, D'Onofrio E, Moreira D (2015) Future sea level rise and changes on tides in the Patagonian Continental Shelf. J Coast Res 31: 519–535.

Mallo C, Fenucci J (2004) Alimentación de protozoeas de langostino *Pleoticus muelleri* utilizando diferentes tipos de microencapsulados y especies de microalgas. Rev Biol Mar Oceanograf 39: 13–19.

Mandelli EF (1965) Contribución al conocimiento de la producción orgánica primaria en aguas Sub-Antárticas (Océano Atlántico Sud-Occidental). An Acad Bras Cienc 37: 399–407.

Mandelli EE, Orlando AM (1966) La producción orgánica primaria y las características fisicoquímicas de la corriente de las Malvinas. Bol Serv Hidrogr Naval 3: 185–196.

Marrari M, Piola AR, Valla D (2017) Variability and 20-year trends in satellite-derived surface chlorophyll concentrations in Large Marine Ecosystems around South and Western Central America. Front Mar Sci doi: 10.3389/fmars.2017.00372.

Matano RP, Palma ED (2018) Seasonal variability of the oceanic circulation in the Gulf of San Jorge, Argentina. Oceanography 31: 16–24.

Menden Deuer S, Lessard EJ (2000) Carbon to volume relationships for dinoflagellates, diatoms, and other protist plankton. Limnol Oceanogr 45: 569–579.

Mitchell BG (1990) Algorithms for determining the absorption coefficient of aquatic particulates using the Quantitative Filter Technique (QFT). In: SPIE, Ocean Optics X, Orlando, Florida.

Moriondo Danovaro, P (2010) Distribución y abundancia de huevos y larvas de langostino patagónico (*Pleoticus muelleri*). Resultados de las campañas estivales AR 01/08 y OB 01/09. Inf Invest INIDEP, N° 19/2010, 13 pp.

Moriondo Danovaro P, Fernández M, Fischbach C, de la Garza J,

Bertuche D (2016) Síntesis de los aspectos biológico-pesqueros del langostino (*Pleoticus muelleri*, Decapoda, Solenoceridae). In: El mar Argentino y sus recursos pesqueros (ed Boschi EE). Tomo 6, INIDEP, Mar del Plata, 95–110.

Odebrecht C, Bergesch M, Rörig L, Abreu P (2010). Phytoplankton interannual variability at Cassino Beach, Southern Brazil (1992–2007), with emphasis on the surf zone diatom *Asterionellopsis glacialis*. Estuar Coast 33: 570–583.

Palma ED, Matano RP, Piola AR (2004) A numerical study of the Southwestern Atlantic Shelf circu-lation: Barotropic response to tidal and wind forcing. J Geophys Res 109: C08014.

Palma ED, Matano RP, Tonini MH, Martos P, Combes V (2020) Dynamical analysis of the oceanic circulation in the Gulf of San Jorge. J Mar Sys 203: 103261.

Pauly D, Christensen, V (1995) Primary production required to sustain global fisheries. Nature 374: 255–257.

Pearl HW (1988) Nuisance phytoplankton blooms in coastal, estuarine, and inland waters. Limnol Oceanogr 33: 823–847.

Pisoni JP, Rivas AL, Tonini MH (2018) Surgencia costera en el Golfo San Jorge. Resúmenes In Jornadas Nacionales de Ciencias del Mar, Buenos Aires, Argentina, 120 pp.

Platt T, Gallegos CL, Harrison WG (1980) Photo inhibition and photosynthesis in natural assemblages of marine phytoplankton. J Mar Res 38: 687–701.

Platt T, Sathyendranath S, Ravindran P (1990) Primary production by phytoplankton: analytic solutions for daily rates per unit area of water surface. Proc Royal Soc Lond 241: 101–111.

Platt, T, Fuentes-Yaco C, Frank K (2003) Marine ecology: Spring algal bloom and larval fish survival. Nature 423: 398–399.

Putt M, Stoecker DK (1989) An experimentally determined carbon: volume ratio for marine "Oligotrichous" ciliates from estuarine and coastal waters. Limnol Oceanogr 34: 1097–1103.

Richardson TL, Jackson GA (2007) Small phytoplankton and carbon export from the surface ocean. Science 315: doi: 10.1126/science.1133471.

Rivas AL, Dogliotti AI, Gagliardini DA (2006) Seasonal variability in satellite-measured surface chlorophyll in the Patagonian shelf. Cont Shelf Res 26: 703–720.

Sabatini M, Martos P (2002) Mesozooplankton features in a frontal area off northern Patagonia (Argentina) during spring 1995 and 1998. Sci Mar 66: 215–232.

Sathyendranath S, Platt T (1988) The spectral irradiance field at the surface and in the interior of the ocean: A model for applications in oceanography and remote sensing. J Geophys Res 93: 9270–9280.

Schlitzer R (2018) Ocean Data View, http://odv.awi.de.

Schloss, IR, Ferreyra ME, Almandoz GO, Codina R, Bianchi A, Balestrini CE, Ochoa HA, Ruiz Pino D, Poisson A (2007) Role of plankton communities in sea-air variation in pCO2 in the SW Atlantic Ocean. Mar Ecol Prog Ser 332: 93–106.

Segura V, Lutz VA, Dogliotti AI, Silva R, Negri R, Akselman R, Benavides H (2013) Phytoplankton types and primary production in the Argentine Sea. Mar Ecol Prog Ser 491: 15–31.

Shannon CE, Weaver W (1949) The mathematical theory of communication. The University of Illinois Press, Urbana, 117 pp.

Sherr E, Sherr B (2007) Heterotrophic dinoflagellates: a significant component of microzooplankton biomass and major grazers of diatoms in the sea. Mar Ecol Prog Ser 352: 187–197.

Sherr E, Sherr B (2009) Capacity of herbivorous protists to control initiation and development of mass phytoplankton blooms. Aquat Microb Ecol 57: 253–262.

Simpson JH (1981) The shelf-sea fronts: implications of their existence and behavior. Phil Trans Roy Soc London A 302: 531–546.

Smetacek V (1985) Role of sinking in diatom life-history cycles: ecological, evolutionary and geological significance. Mar Biol 84: 239–251.

Sosik HM, Mitchell BG (1995) Light absorption by phytoplankton, photosynthetic pigments and detritus in the California Current System. Deep-Sea Res 42: 1717–1748.

Souto VS, Moriondo Danovaro PI (2019) Distribución y densidad de huevos y larvas de langostino patagónico (*Pleoticus muelleri*) en el frente de Península Valdés. Resultados de la campaña VA15/18. Inf Invest 91: 13 pp.

Throndsen J (1978) Preservation and storage. In: Phytoplankton manual (ed Sournia A). Unesco monographs on oceanographic methodology, Paris, 69–74.

Tomas CR (1997) Identifying marine phytoplankton. Academic Press, 858 pp.

Tonini MH, Palma ED, Rivas AL (2006) Modelo de alta resolución de los golfos norpatagónicos. Mecánica Computacional 25: 1441–1460.

Verity PG, Sieracki ME (1993) Use of color image analysis and epifluorescence microscopy to measure plankton biomass. In: Handbook of Methodology in Aquatic Microbial Ecology (Kemp PF, Sherr BF, Sherr EB, Cole JJ eds). Lewis Publishers, Boca Raton, pp. 187–197.

Villafañe VE, Barbini E, Helbling EW (2004a) Annual patterns of ultraviolet radiation effects on temperate marine phytoplankton off Patagonia, Argentina. J Plankton Res 26: 167–174.

Villafañe VE, Marcoval A, Helbling EW (2004b) Photosynthesis versus irradiance characteristics in phytoplankton assemblages off Patagonia (Argentina): temporal variability and solar UVR effects. Mar Ecol Prog Ser 284: 23–34.

Williams GN, Larouche P, Dogliotti AI, Latorre MP (2018) Light absorption by phytoplankton, non algal particles and dissolved organic matter in San Jorge Gulf in summer. Oceanography 31: 40–49.

Wyngaard JG, Iorio MI, Firpo C (2016) Los crustáceos de interés pesquero y otras especies relevantes en los ecosistemas marinos. In: El Mar Argentino y sus Recursos Pesqueros (ed Boschi EE). Tomo 6, INIDEP, Mar del Plata, 271 pp.